

# Mechanical properties of amorphous nanosprings

Alexandre F. da Fonseca<sup>1</sup>, C. P. Malta<sup>1</sup> and D. S. Galvão<sup>2</sup>

<sup>1</sup> Instituto de Física, Universidade de São Paulo, Caixa Postal 66318, 05315-970, São Paulo, Brazil

<sup>2</sup> Instituto de Física 'Gleb Wataghin', Universidade Estadual de Campinas, Unicamp 13083-970, Campinas, SP, Brazil

E-mail: [afonseca@if.usp.br](mailto:afonseca@if.usp.br), [coraci@if.usp.br](mailto:coraci@if.usp.br), [galvao@ifi.unicamp.br](mailto:galvao@ifi.unicamp.br)

## Abstract.

Helical amorphous nanosprings have attracted particular interest due to their special mechanical properties. In this work we present a simple model, within the framework of the Kirchhoff rod model, to investigate the structural properties of nanosprings having asymmetric cross section. We have derived expressions that can be used to obtain the Young's modulus and Poisson's ratio of the nanospring material composite. We also address the importance of the presence of a catalyst in the growth process of amorphous nanosprings in terms of the stability of helical rods.

PACS numbers: 62.25.+g, 61.46.+w, 46.70.Hg

Submitted to: *Nanotechnology*

## 1. Introduction

Nowadays, one of the most important challenges in Science is the complete characterization of all physical and chemical properties of structures at nanoscale. Since the Iijima's seminal paper reporting the discovery of carbon nanotubes [1], the interest of the scientific community in nanostructured materials has exponentially increased due to their great potential in technological applications [2, 3, 4, 5, 6, 7, 8]. This has motivated the development of several processes for growing nanostructures.

Helical nanowires, or simply *nanosprings*, are particularly interesting one-dimensional nanostructures [9] due to their special periodic and elastic properties. Examples of such structures are quasi-nanosprings [10], helical crystalline nanowires [11, 12, 13] and amorphous nanosprings [14, 15, 16].

Volodin *et al* [17] have studied the elastic properties of helix-shaped nanotubes using Atomic Force Microscopy (AFM). They used a circular beam approximation to model the elastic response of a single winding of coiled nanotube. Recently, Chen *et al* [18] measured the spring constant of carbon nanocoils and used a classical approach which relates the spring constant to the shear modulus of the composite material.

In this paper, we present a model that can be used by experimentalists to determine the elastic properties of different amorphous nanosprings. Our calculations are based on the Kirchhoff rod model [19] that provides a framework to study statics and dynamics of thin elastic filaments. The static Kirchhoff equations will be used to derive expressions for the Young's modulus and the Poisson's ratio of the nanospring material composite. The nanowire here is assumed to have elliptic cross section, so the present work constitutes an extension of our previous works [20, 21] for nanowires with circular cross-section.

It is known that the synthesis of amorphous nanowires and nanosprings requires the presence of a metallic catalyst. Following the vapor-liquid-solid (VLS) growth model, known since 1964 [22] for whisker formation, a liquid droplet of a metal absorbs a given material from the surrounding vapor, and after super-saturation of the absorbed material within the droplet, the excess material precipitates at the liquid-solid interface forming the nanowire beneath the metallic droplet.

McIlroy *et al* [9, 14] developed a modified VLS growth model to explain the formation of amorphous nanosprings based on the interactions between the metallic catalyst and the nanowire. The interesting feature is that the modified VLS growth model [9] does not depend on the composite material of the nanospring and, therefore, it can be applied to any type of amorphous nanosprings.

Here, we will take advantage of the modified VLS growth model proposed by McIlroy *et al* [9] to analyse an important mechanical consequence of the presence of the metallic catalyst in the growth process of amorphous nanosprings. We show that the asymmetric growth driven by the metallic catalyst provides the nanowire with a *helical intrinsic curvature* which is required to maintain it dynamically stable.

The Kirchhoff model [19] has been extensively used to model the structure and

elasticity of long DNA chains [23, 24, 25, 26, 27, 28, 29], the tendrils of climbing plants [30, 31], slender cables subject to different stresses [32], etc. The Kirchhoff model is also appropriate for investigating the elastic properties of amorphous helical nanostructures.

For nanowires with elliptic cross-section, there are two types of helical structures, *normal* and *binormal*. In Section II, we present the Kirchhoff rod model and, for each type of helix, derive two expressions that can be used to obtain the Young's modulus and the Poisson's ratio of an amorphous nanospring composite material. One of expressions relates the Hooke's constant to the Young's modulus, and to the geometric features of the nanospring. The other expression relates an applied torque in the direction of the helical axis of the nanospring, to the Young's modulus and Poisson's ratio of the material. We have used the measured Hooke's constant for a carbon nanocoil, reported in Ref. [18], to test the expression for the Young's modulus. In Section III we analyse the stability of helical filaments, and show that the presence of a metallic catalyst has important consequences in the growth process of nanosprings. In section IV we summarize our results and conclusions.

## 2. The elastic model

In this section, we derive two expressions that can be used by experimentalists to obtain the elastic constants of the composite material of amorphous nanosprings. Both expressions involve two geometric parameters that define a helical space curve, namely, the *curvature*,  $\kappa$ , and the *torsion*,  $\tau$ .

We shall first briefly describe a helical curve and its relation to the curvature and torsion. Then, we present the Kirchhoff rod model, that is used to derive the above mentioned expressions for studying the elastic properties of amorphous nanosprings.

### 2.1. Helical space curve

A space curve  $\mathbf{x}$  is a *helix* if the lines tangent to  $\mathbf{x}$  make a constant angle with a fixed direction in space (the helical axis) [33].

A helical space curve  $\mathbf{x}$  can be expressed in a fixed Cartesian basis as:

$$\mathbf{x} = R \cos(\lambda s) \mathbf{e}_x + R \sin(\lambda s) \mathbf{e}_y + \frac{P}{2\pi} \lambda s \mathbf{e}_z, \quad (1)$$

where

$$\lambda = \sqrt{\frac{1}{(R^2 + \frac{P^2}{4\pi^2})}}, \quad (2)$$

$R$  is the radius of the helix, and  $P$  is the *pitch* of the helix, i.e, the distance between two adjacent loops.  $\{\mathbf{e}_x, \mathbf{e}_y, \mathbf{e}_z\}$  is a fixed Cartesian basis where  $\mathbf{e}_z$  is chosen along the direction of the axis of the helix. Fig. 1 shows a helical filament of radius,  $R$ , and pitch,  $P$ .

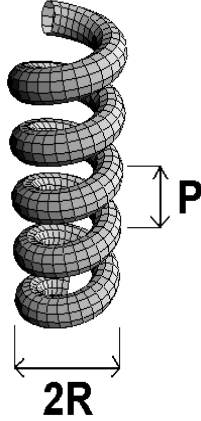


**Figure 1.** A helical rod characterized by a radius  $R$  and a loop-to-loop distance  $P$ .

The radius,  $R$ , and pitch,  $P$ , of the helix are related to the curvature,  $\kappa$ , and torsion,  $\tau$ , through:

$$\begin{aligned}\kappa &= R\lambda^2, \\ \tau &= \frac{P}{2\pi}\lambda^2.\end{aligned}\tag{3}$$

In terms of  $\kappa$  and  $\tau$ , the helical curve  $\mathbf{x}$  can be written as [31]:

$$\mathbf{x} = \frac{\kappa}{\lambda^2} \cos(\lambda s) \mathbf{e}_1 + \frac{\kappa}{\lambda^2} \sin(\lambda s) \mathbf{e}_2 + \frac{\tau}{\lambda} s \mathbf{e}_3,\tag{4}$$

where  $\lambda$  can also be written in terms of  $\kappa$  and  $\tau$  by:

$$\lambda = \sqrt{\kappa^2 + \tau^2}.\tag{5}$$

These equations will be useful to derive the relations for the elastic constants of the nanospring.

## 2.2. The Kirchhoff rod model

In Kirchhoff's theory, the rod is seen as an assembly of short segments loaded by contact forces from the adjacent ones. The classical equations for the conservation laws of linear and angular momentum are applied to each segment in order to obtain a one dimensional set of differential equations for the static and dynamics of the rod in the approximation of large radius of curvature and large total length of the rod as compared to the radius of the local cross-section [34]. These equations contain the forces and torques, plus a triad of vectors describing the deformations of the rod. In this paper, we shall be concerned only with static solutions and, therefore, only the static Kirchhoff equations will be presented:

$$\mathbf{F}' = 0,\tag{6}$$

$$\mathbf{M}' + \mathbf{d}_3 \times \mathbf{F} = 0,\tag{7}$$

where  $\mathbf{F}$  and  $\mathbf{M}$  are the total force and torque across the cross-sections of the rod, respectively.  $\mathbf{d}_3$  is the vector tangent to the centerline or the axis of the rod. The prime denotes the derivative with respect to the arc-length  $s$  of the rod. In order to solve the equations we introduce the constitutive relationship from linear elasticity theory [34] that, for a rod with elliptic cross-section, is given by [35]:

$$\mathbf{M} = EI_1(k_1 - k_1^{(0)})\mathbf{d}_1 + EI_1a(k_2 - k_2^{(0)})\mathbf{d}_2 + EI_1b(k_3 - k_3^{(0)})\mathbf{d}_3, \quad (8)$$

where  $E$  is the Young's modulus,  $a \equiv I_2/I_1$ , with  $I_1$  and  $I_2$  being the principal moments of inertia of the cross section in the directions of  $\mathbf{d}_1$  and  $\mathbf{d}_2$ , respectively, with  $I_1 \geq I_2$ . Since the bending coefficient of the rod is proportional to the moment of inertia, the vectors  $\mathbf{d}_1$  and  $\mathbf{d}_2$  represent the directions of greatest and lowest bending stiffness of the rod, respectively.  $a$ ,  $0 < a \leq 1$ , measures the bending asymmetry of the cross section.  $\mathbf{d}_1$  and  $\mathbf{d}_2$  lie in the plane of the cross section so that  $\{\mathbf{d}_1, \mathbf{d}_2, \mathbf{d}_3\}$  forms a right handed director basis defined at each point along the axis of the rod. The constant  $b$  is called *scaled torsional stiffness* and for a rod of elliptic cross-section with semiaxes  $A$  and  $B$  ( $A < B$ ),  $a$  and  $b$  are given by [35, 36, 37]:

$$a = \frac{A^2}{B^2}, \quad b = \frac{1}{1 + \sigma} \frac{2a}{1 + a}. \quad (9)$$

where  $\sigma$  is the Poisson's ratio of the material.

$k_j$ ,  $j = 1, 2, 3$ , are the components of the so-called *twist vector*,  $\mathbf{k}$ , which defines the variation of the director basis  $\{\mathbf{d}_1, \mathbf{d}_2, \mathbf{d}_3\}$  with the arc-length  $s$  through the expression:

$$\mathbf{d}'_j = \mathbf{k} \times \mathbf{d}_j, \quad j = 1, 2, 3. \quad (10)$$

$k_1$  and  $k_2$  are related to the curvature  $\kappa$  of the centerline of rod through  $\kappa = \sqrt{k_1^2 + k_2^2}$ , and  $k_3$  is the twist density of the rod.  $k_j^{(0)}$ ,  $j = 1, 2, 3$ , defines the variation of the director basis of the rod in its unstressed configuration.  $k_j^{(0)}$ ,  $j = 1, 2, 3$ , represent the *intrinsic curvature* of the rod, which is the tridimensional configuration displayed by the rod when it is free from stresses.

The Kirchhoff equations (6-8) admit two types of helical solutions for rods with elliptic cross section, called *normal* and *binormal* helices. A helical solution is represented by a set of expressions for the twist vector and the force, and the upper index  $n$  ( $b$ ) will be used to denote normal (binormal) helical solutions. Figure 2 displays an example of these types of helix. The normal helix solution is given by:

$$\mathbf{k}^n = \kappa\mathbf{d}_1 + \tau\mathbf{d}_3, \quad (11)$$

$$\mathbf{F}^n = \gamma_1\tau\mathbf{k}^n. \quad (12)$$

The binormal helix solution is given by:

$$\mathbf{k}^b = \kappa\mathbf{d}_2 + \tau\mathbf{d}_3, \quad (13)$$

$$\mathbf{F}^b = \gamma_2\tau\mathbf{k}^b. \quad (14)$$

where  $\kappa$  (*curvature*) and  $\tau$  (*torsion*) are the geometric parameters of the space curve defined by the helical axis of the rod, and

$$\gamma_i = b\left(1 - \frac{\tau_0}{\tau}\right) - [1 + (a - 1)\delta_{i2}]\left(1 - \frac{\kappa_0}{\kappa}\right), \quad i = 1, 2. \quad (15)$$

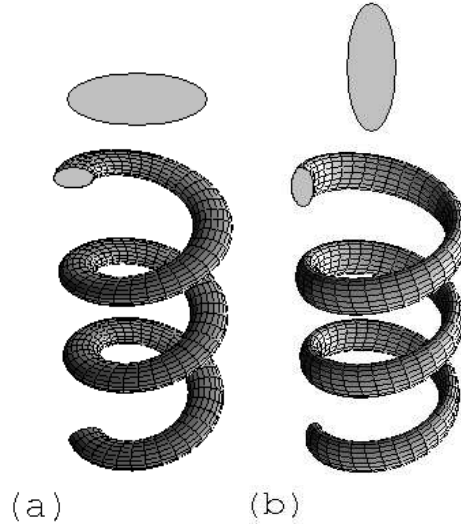


**Figure 2.** Normal (a) and binormal (b) helices and the corresponding orientated cross-sections.

where  $\kappa_0$  and  $\tau_0$  are the *intrinsic* curvature and torsion of the helical structure ( $\mathbf{k}^{(0)} = \kappa_0 \mathbf{d}_i + \tau_0 \mathbf{d}_3$ ),  $i = 1$  ( $i = 2$ ) for a normal (binormal) helix.  $\delta_{i2}$  is the Kronecker delta.

We can relate the director basis,  $\{\mathbf{d}_1, \mathbf{d}_2, \mathbf{d}_3\}$ , to the fixed Cartesian basis,  $\{\mathbf{e}_x, \mathbf{e}_y, \mathbf{e}_z\}$ , integrating the eq. (10) using the eqs. (11) and (13) for normal and binormal helices, respectively. We obtain the following relations:

$$\mathbf{d}_1^n = \frac{1}{\lambda} (\tau \sin(\lambda s) \mathbf{e}_x - \tau \cos(\lambda s) \mathbf{e}_y + \kappa \mathbf{e}_z), \quad (16)$$

$$\mathbf{d}_2^n = \cos(\lambda s) \mathbf{e}_x + \sin(\lambda s) \mathbf{e}_y, \quad (17)$$

$$\mathbf{d}_3^n = \frac{1}{\lambda} (-\kappa \sin(\lambda s) \mathbf{e}_x + \kappa \cos(\lambda s) \mathbf{e}_y + \tau \mathbf{e}_z), \quad (18)$$

for the normal helix, and

$$\mathbf{d}_1^b = \sin(\lambda s) \mathbf{e}_x + \cos(\lambda s) \mathbf{e}_y, \quad (19)$$

$$\mathbf{d}_2^b = \frac{1}{\lambda} (\tau \cos(\lambda s) \mathbf{e}_x - \tau \sin(\lambda s) \mathbf{e}_y + \kappa \mathbf{e}_z), \quad (20)$$

$$\mathbf{d}_3^b = \frac{1}{\lambda} (-\kappa \cos(\lambda s) \mathbf{e}_x + \kappa \sin(\lambda s) \mathbf{e}_y + \tau \mathbf{e}_z), \quad (21)$$

for the binormal helix. Since  $\mathbf{d}_3 = \mathbf{x}'$  we can integrate eqs. (18) and (21) to obtain an expression for  $\mathbf{x}$  similar to the eq. (4), except for a difference in phase.

From eqs. (12) and (14) we can obtain the total tension force  $T$  along the direction of the axis of the helix (here defined as  $\mathbf{e}_z$ ):

$$T = \mathbf{F} \cdot \mathbf{e}_z = \gamma_i \tau \mathbf{k} \cdot \mathbf{e}_z, \quad i = 1, 2, \quad (22)$$

where  $\gamma_i$  is given by eq. (15) and  $i = 1$  ( $i = 2$ ) is related to the vectors  $\mathbf{F}$  and  $\mathbf{k}$  for the normal (binormal) helix given by eqs. (11) (eqs. (13)). Since the twist vector  $\mathbf{k}$

is written in the director basis through eq. (11) (eq. (13)), we can use eqs. (16) (eqs. (19)) to obtain  $T$ :

$$T = \frac{EI_1}{L^2} \gamma_i L^2 \tau \lambda = EI_1 \gamma_i \tau \lambda, \quad i = 1, 2, \quad (23)$$

where the terms  $EI_1/L^2$  and  $L^2$  appeared in accord to the following conversion to unscaled variables:

$$T \rightarrow \frac{L^2}{EI_1} T, \quad \kappa \rightarrow L\kappa, \quad \tau \rightarrow L\tau \quad \text{and} \quad \lambda \rightarrow L\lambda, \quad (24)$$

with  $L$  being a length scale of the rod that, in our case, is chosen to be the arc-length of one loop of the unstressed helical rod:  $L = 2\pi/\lambda_0$  with  $\lambda_0 = \sqrt{\kappa_0^2 + \tau_0^2}$ .  $E$  is the Young's modulus of the composite material of the rod, and  $I_1$  is the moment of inertia along  $\mathbf{d}_1$  (it is the direction of the greatest bending stiffness). For an elliptic cross section of semiaxes  $A$  and  $B$  ( $A < B$ ),  $I_1$  is given by:

$$I_1 = \frac{B^3 A \pi}{4}. \quad (25)$$

### 2.3. Expressions for the elastic constants of the nanospring

McMillen and Goriely [31] used the Kirchhoff model to obtain an expression for the Hooke's constant  $h$  of a helix, with intrinsic curvature  $\mathbf{k}^{(0)} = \kappa_0 \mathbf{d}_1 + \tau_0 \mathbf{d}_2$ , in terms of the properties of the rod's material, the Young's modulus, and the moment of inertia of the circular cross-section.

Here, we follow the same steps to derive an expression for the Hooke's constant of a helical filament with elliptic cross section. We also derive an expression relating a torque applied along the direction of the helical axis, to the Poisson's ratio of the helical filament.

Consider a helical rod in its unstressed state represented by  $\mathbf{k}^{(0)} = \kappa_0 \mathbf{d}_i + \tau_0 \mathbf{d}_3$ ,  $i = 1$  ( $i = 2$ ) for normal (binormal) intrinsically helical configuration. The ends of the rod are held fixed so that they do not rotate as the applied tension at the ends is changed. Since the ends do not rotate, it imposes a constraint in the total twist  $T_W$  of the rod:

$$T_W \equiv \int k_3 ds = \int \tau_0 ds = \int \tau ds. \quad (26)$$

The consequence of this constraint is that the torsion  $\tau$  remains constant ( $\tau = \tau_0$ ) for the tensioned helical rod.

Consider two material points,  $Q_1$  and  $Q_2$ , in the unstressed configuration, that are located at arc-length positions  $s_1 = 0$  and  $s_2 = 2\pi/\lambda_0$ , respectively.  $2\pi/\lambda_0$  is exactly the arc-length of one loop of the unstressed helical configuration. When a tension is applied to the rod, the distance between those points  $Q_1$  and  $Q_2$ , along the helix axis, is given by  $d = z(2\pi/\lambda_0) - z(0)$ . Using eq. (4),  $d$  can be written as

$$d = \frac{2\pi\tau}{\lambda\lambda_0}, \quad (27)$$

where  $\lambda$  and  $\tau$  are related to the deformed (stretched or compressed) helical structure. From (27), we obtain the expression for  $\tau$ :

$$\tau = \tilde{d}\lambda, \quad (28)$$

where  $\tilde{d}$  is the dimensionless distance

$$\tilde{d} \equiv \frac{d}{L} = d \frac{\lambda_0}{2\pi}. \quad (29)$$

The eq. (15) can be simplified for this case where  $\tau = \tau_0$ :

$$\gamma_i = [1 + (a - 1)\delta_{i2}] \left( \frac{\kappa_0}{\kappa} - 1 \right), \quad i = 1, 2. \quad (30)$$

Substituting eq. (30) in eq. (23) we obtain the following expression for the tension  $T$ :

$$T = EI_1[1 + (a - 1)\delta_{i2}] \left( \frac{\kappa_0}{\kappa} - 1 \right) \tau \lambda, \quad i = 1, 2. \quad (31)$$

From the relation (5), using eq. (28), we obtain

$$\kappa = \sqrt{\lambda^2 - \tau^2} = \lambda \sqrt{1 - \tilde{d}^2}. \quad (32)$$

Substituting eq. (32) in eq. (31), and using eq. (28), we obtain an expression for  $T$  as function of  $\tilde{d}$ :

$$T = EI_1[1 + (a - 1)\delta_{i2}] \left( \frac{\kappa_0 \tau}{\sqrt{1 - \tilde{d}^2}} - \frac{\tau^2}{\tilde{d}} \right), \quad i = 1, 2. \quad (33)$$

If  $\tilde{d}_0$  is the distance between the points  $Q_1$  and  $Q_2$  in the unstressed configuration of the rod, then  $\tilde{d} = \tilde{d}_0 = \tau_0/\lambda_0$  when no tension is applied to the rod. Eq (33) shows that the tension  $T$  varies from 0 to  $\infty$  if  $\tilde{d}$  varies from  $\tilde{d}_0$  to 1. In order to find the Hooke's constant,  $h$ , of the tensioned helical rod, we consider a small variation of  $\tilde{d}$  defined by the small displacement  $\hat{d}$ , i.e., we let  $\tilde{d} = \tilde{d}_0 + \hat{d}$ ,  $\hat{d} \ll 1$ . Then we look for an expression for the Hooke's constant such that:

$$T = h\hat{d} + O(\hat{d}^2). \quad (34)$$

Expanding eq. (33) for a small variation of  $\tilde{d}$  around  $\tilde{d}_0$ , we obtain

$$T = EI_1[1 + (a - 1)\delta_{i2}] \lambda_0^2 \left( 1 + \frac{\tau_0^2}{\kappa^2} \right) \hat{d} + O(\hat{d}^2), \quad i = 1, 2. \quad (35)$$

For a spring with  $N$  coils, its displacement due to the action of a given tension  $T$  is obtained replacing  $\{\hat{d}\}$  by  $\left\{ \frac{\hat{d}}{NL} \right\}$  in the above equation where, now,  $\hat{d}$  is written in unscaled units. It gives the following final expression for the Hooke's constant,  $h$ :

$$h = \frac{EI_1}{2\pi N} [1 + (a - 1)\delta_{i2}] \lambda_0^3 \left( 1 + \frac{\tau_0^2}{\kappa^2} \right), \quad i = 1, 2, \quad (36)$$

where  $i = 1$  ( $i = 2$ ) refers to the normal (binormal) helix solution. By making  $a = 1$  we recover our previous result [20] for the Hooke's constant of a nanospring made of a nanowire with circular cross section.

Eq. (36) relates the Hooke's constant,  $h$ , to the Young's modulus,  $E$ , of the material composite of the nanospring, to the moment of inertia,  $I_1$ , and to the geometric

parameters  $\kappa_0$ ,  $\tau_0$ ,  $\kappa$  and  $\lambda_0 = \sqrt{\kappa_0^2 + \tau_0^2}$ . The moment of inertia,  $I_1$ , and the parameter  $a$  can be obtained by measuring the semiaxes  $A$  and  $B$  of the elliptic cross section of the nanowire and using Eqs. (25) and (9), respectively. The geometric parameters can be obtained by measuring the radius,  $R$ , and the pitch,  $P$ , of the nanospring and using the eqs. (2) and (3) that relates  $R$  and  $P$  to  $\lambda$ ,  $\kappa$  and  $\tau$ . In order to obtain the values of the geometric parameters of the unstressed configuration, we must measure  $R_0$  and  $P_0$  of the unstressed helical configuration, and then use the eqs. (2) and (3) to obtain  $\lambda_0$ ,  $\kappa_0$  and  $\tau_0$ . Therefore, by measuring the Hooke's constant of the nanospring we can use eq. (36) to obtain the Young's modulus of the composite material of the nanospring. Figure 3 shows a scheme that can be used for measuring the Hooke's constant of the nanospring.

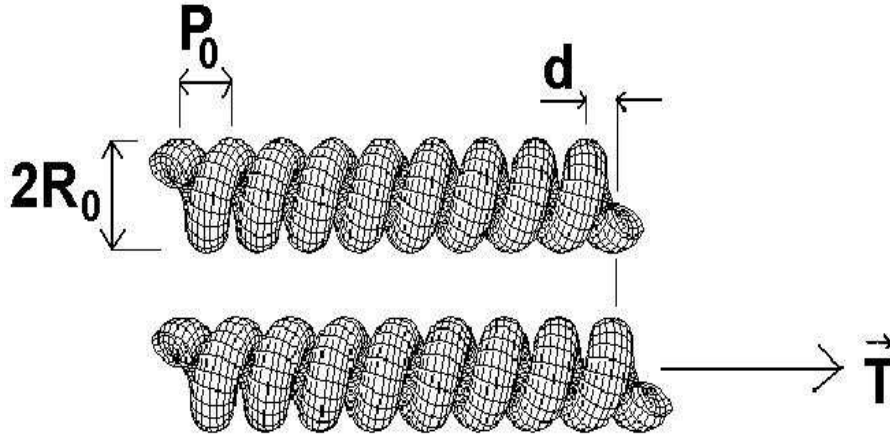


**Figure 3.** Outline of the experiment to measure the Hooke's constant,  $h$ .  $R_0$  and  $P_0$  are the radius and the pitch of the helix in the unstressed configuration. The helix shown corresponds to a nanospring of radius  $R_0 = 51\text{nm}$  and  $P_0 = 85\text{nm}$ .

We, now, derive an expression to obtain the Poisson's ratio  $\sigma$  of the nanospring. We depart from the eq. (8) for the total torque across each cross section, and then use eq. (11) (eq. (13)) for the components of the twist vector  $\mathbf{k}$  for a normal (binormal) helix. Basically, we want to obtain the axial component of the torque  $M_Z \equiv \mathbf{M} \cdot \mathbf{e}_z$ . Using eqs. (16) and (19) we obtain the following expression for  $M_Z$ :

$$M_Z = [1 + (a - 1)\delta_{i2}](\kappa - \kappa_0)\frac{\kappa}{\lambda} + b(\tau - \tau_0)\frac{\tau}{\lambda}, \quad i = 1, 2, \quad (37)$$

where  $i = 1$  ( $i = 2$ ) corresponds to a normal (binormal) helical nanospring.

Eq. (37) can be used to obtain, experimentally, the Poisson's ratio  $\sigma$  of the nanospring. Figure 4 shows a scheme to obtain the Poisson's ratio. Measuring the radius,  $R_1$ , and the pitch,  $P_1$ , of the stressed helix,  $\kappa$  and  $\tau$  can be obtained from eqs. (2) and (3). By measuring the applied torque in the direction of the axis of the helix,  $M_Z$ , we can use the Eq. (37) to obtain the parameter  $b$ . The values of  $a$ ,  $\kappa_0$ ,  $\tau_0$ ,  $I_1$  and the nanospring Young's modulus are needed to obtain  $b$ . The Poisson's ratio,  $\sigma$ ,

can, therefore, be obtained using the Eq. (9). In this experimental scheme, both ends of the nanospring must be held fixed in order to avoid relaxation.

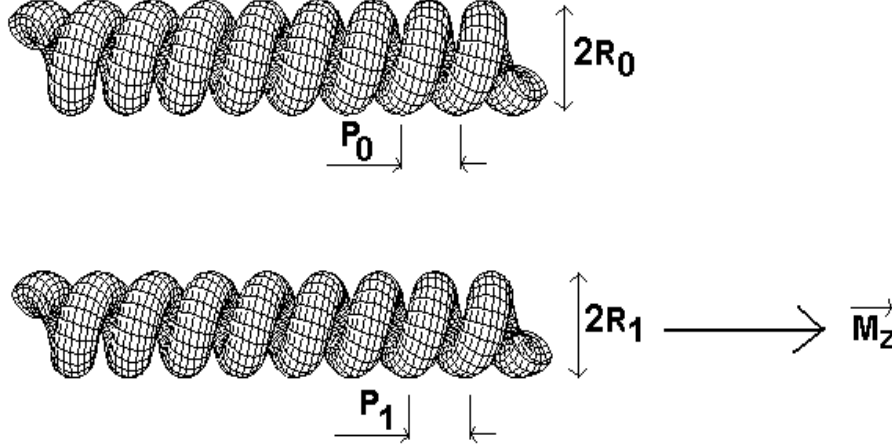


**Figure 4.** Outline of the experiment to measure the Poisson's ratio  $\sigma$ . The extremities of the nanospring must be held fixed. See the text for the details.

We can test the equation (36) using the parameters for a unit nanocoil ( $N = 1$ ) considered by Chen *et al* [18]: the diameter of the nanowire  $D = 120\text{nm}$ , the radius of the helix  $R = 420\text{nm}$  and the pitch of the helix  $P = 2000\text{nm}$ . The material has a Poisson's ratio  $\sigma = 0.27$  and a shear modulus  $\mu = 2.5\text{GPa}$ . The amorphous carbon nanocoil used by Chen *et al* is, in fact, a double coil formed by two wires tightly joined [18, 38], as indicated by scanning electron microscope (SEM) and transmission electron microscope (TEM) images depicted in Figure 7 of Reference [18]. In order to test our model, we shall approximate the carbon nanocoil by a homogeneous rod with circular cross section of diameter  $D$ .

Assuming that the rod has circular cross section, eq. 9 gives  $a = 1$  and  $b = (1 + \sigma)^{-1} = 2\mu/E$ . Using the values given above for  $\mu$  and  $\sigma$ , we obtain that the nanocoil material has the Young's modulus  $E_{bulk} = 6.35\text{GPa}$ .

Now, using the equations (2) and (3) we obtain  $\kappa_0$  and  $\tau_0$  of the carbon nanocoil from the values of  $R$  and  $P$  given above. Then, using the measured Hooke's constant of the nanocoil,  $h = 0.12\text{N/m}$  [18], the Eq. (36), with  $a = 1$  (circular cross section), and  $N = 1$  (unit nanocoil), gives  $E_{nanocoil} \simeq 6.88\text{GPa}$ , which is slightly larger than  $E_{bulk} = 6.35\text{GPa}$ . A possible explanation for these different results would be that the nanowire cross section is not circular. In the Conclusion we comment further on this point.

As for Eq (37), it cannot be tested for lack of experimental measurements of the axial torque of a nanospring.

### 3. Mechanical function for the catalyst

McIlroy *et al* [9, 14] have proposed a model of nanospring formation based upon the vapour-liquid-solid (VLS) growth mechanism by Wagner and Ellis [22]. The key feature of the VLS model is the presence of a liquid catalyst that absorbs the material from surrounding vapour and, after becoming supersaturated, the material is deposited beneath the catalyst-substrate interface, thereby forming the nanowire [9, 14].

The basic characteristics required for the nanowire formation are the temperature of the catalyst, that must be higher than its melting point (if the catalyst is not liquid, the material in the vapour cannot be absorbed), and the vapour material, that must be soluble in the liquid catalyst [9]. Also, the geometry of the liquid catalyst has a strong influence on the geometry of the growing nanowire and this feature was explored by McIlroy *et al* in their modified VLS growth model for nanosprings.

We shall show that, from the mechanical point of view, the metallic catalyst has an important role in the growth process of amorphous nanosprings through the VLS mechanism. Our analysis shows that the McIlroy *et al* VLS growth model is consistent with the mechanical stability of the grown helical structures.

Goriely and Tabor developed a dynamical method to test the stability of equilibrium solutions of the Kirchhoff model [39, 40]. They showed [41] that helices with intrinsic curvature ( $\kappa_0 \neq 0$  and  $\tau_0 \neq 0$ ) do not admit unstable modes being, therefore, dynamically stable.

McMillen and Goriely [31] have studied how differential growth can affect the intrinsic curvature of biological materials as the climbing plants. According to the modified VLS growth model for nanosprings, the asymmetric geometric features of the catalytic particle induce a differential growth, during the process of formation of the helical nanowire. This differential growth produces the helical intrinsic curvature thus conferring dynamical stability to the forming nanospring. It is a desirable feature because the growth process is very sensitive to diverse characteristics of the system as the temperature of the catalyst, the pressure of the vapour, etc. Therefore, from the mechanical point of view, the asymmetric growth is a self-sustained process.

Goriely and Shipman [35] studied the dynamics of elastic helical thin rods with noncircular cross section. They concluded that a finite helical binormal strip, clamped at both ends, is dynamically stable if its cross section is flat, *i.e.*, if  $A \ll B$  (Eq. (9)).

Basically, the asymmetric growth occurs due to the interaction between the surface tension between the liquid-vapour ( $\gamma_{LV}$ ), solid-vapour ( $\gamma_{SV}$ ) and solid-liquid ( $\gamma_{SL}$ ) interfaces. McIlroy *et al* [9, 14] proposed that the growth process occurs due to the contact angle anisotropy (CAA) at the catalyst-nanowire interface. The work required to shear the catalyst from the nanowire is called the thermodynamic work of adhesion  $W_A$  and can be computed in terms of the surface tensions by [9]:

$$\begin{aligned} W_A &= \gamma_{SV} + \gamma_{SL} - \gamma_{LV} \\ &= \gamma_{SV}(1 - \cos \theta) \end{aligned} \quad (38)$$

where  $\theta$  is the angle between the surface tensions  $\gamma_{SL}$  and  $\gamma_{SV}$ . The CAA is responsible

for the differential growth resulting in the dynamical stability to the forming nanospring.

#### 4. Conclusions

The Kirchhoff rod model has been used to obtain a simple model to investigate the elastic properties of amorphous nanosprings. We derived the expressions (36) and (37) that can be used to obtain the Young's modulus and the Poisson's ratio of the composite material of a nanospring. These expressions relate the material elastic constants to the geometric features of the nanowire helical structure, and cross section.

We have considered the case of nanowire with elliptic cross section that leads to two types of helical solutions for the Kirchhoff equations: normal and binormal helices (Fig. 2). In the particular case of nanowire with circular cross section, we recover the expressions derived in Ref. [20].

Figures 3 and 4 display our proposed schemes for measuring the Hooke's constant, and the applied torque along the direction of the axis of the helix, together with the radius,  $R$ , and the pitch,  $P$ , of the helical structure. Using Eqs. (2) and (3) we can obtain the curvature,  $\kappa$ , and torsion,  $\tau$ , of the nanospring, and using Eqs. (36) and (37), we obtain the Young's modulus and the Poisson's ratio of the nanospring.

Applying (36) to the unit carbon nanocoil used by [18], we obtained the nanocoil Young's modulus  $E_{nanocoil}$  larger than  $E_{bulk}$ , which could be due to the nanocoil having non-circular cross section. Nevertheless, we should point out that experimentalists have observed that the measured Young's modulus and Poisson's ratio of nanostructures are different from those of the bulk material. For instance, Salvadori *et al* found that the Young's modulus of gold thin film is about 12% smaller than that of the bulk material [42, 43]. Using alternating electrical fields, Dikin *et al* [44] excited bending vibrations in SiO<sub>2</sub> nanowires to measure their Young's modulus, obtaining values smaller than that of the bulk SiO<sub>2</sub> material. In another example, Cuenot *et al* [45] used the effects of surface tension in bent structures to explain the larger values of the Young's modulus observed in nanowires with smaller diameters. It is important to investigate when the Young's modulus, and the Poisson's ratio of the nanostructure start to deviate from those of the bulk material.

Eq. (37) gives the torque required to twist a nanospring (having curvature  $\kappa_0$ , and torsion  $\tau_0$ , in the unstressed configuration) so as to produce a new helical structure with curvature  $\kappa$ , and torsion  $\tau$ . It is important to stress that Eq. (37) depends on the Young's modulus, and Poisson's ratio of the nanospring, therefore, by measuring  $M_Z$ , it is possible to determine one of these elasticity parameters if the other is known. We have not been able to apply Eq. (37) for lack of experimental measurements of  $M_Z$ .

Using the stability analysis developed by Goriely and Tabor [39, 40, 41], we have concluded that the presence of the catalytic particle is very important to the growth process of nanowires and nanosprings. From the mechanical point of view, the catalyst promotes the differential growth that provides dynamical stability to the helical nanowire, making the growth process self-sustained. This result shows the consistency

of the modified VLS growth model proposed by McIlroy *et al* [9, 14] to explain the formation of amorphous nanosprings.

The importance of the presence of the metallic catalyst, in the growth process of nanospring, is corroborated by the analysis of a recent report on spontaneous polarization-induced growing of nanosprings and nanorings of piezoelectric zinc oxide (ZnO) by Kong and Wang [13]. Their crystalline nanosprings were produced without the presence of catalytic particles. They found that the mechanism for the helical growth is the consequence of minimizing the total energy contributed by spontaneous polarization and elasticity. The electrostatic forces between the polarized material and the substrate play the role of an external force holding the rod in the helical shape. If these helical nanostructures were taken away from the substrate, the electrostatic forces would cease and the nanostructure would release its elastic energy becoming straight, implying that these nanostructures do not have intrinsic helical curvature. This is an indirect evidence that supports the modified VLS growth where the particles drive an asymmetric growth, thus providing the necessary dynamical stability to the uniform growth. This example highlights the importance of the relationship between the metallic catalyst and the dynamical stability of the nanosprings.

Our results may open up new possible technological applications depending on the type of helical nanostructure. Eq. (36) shows that, for a given geometry of the nanowire cross section, the Hooke's constant of the normal helical configuration is always higher than that of the binormal one. It indicates that it is possible to produce identical helices (same curvature and torsion) with different elastic properties, that may be useful in nanoelectromechanical systems.

## Acknowledgments

This work was partially supported by the FAPESP, CNPq, IMMP, IN, SAMNBAS and FINEP.

## References

- [1] Iijima S 1991 *Nature* (London) **354** 56.
- [2] Baughman R H, Zakhidov A A and de Heer W A 2002 *Science* **297** 787.
- [3] Samuelson L 2003 *Mater. Today* **6**(10) 22.
- [4] Ratner M A and Ratner D 2002 *Nanotechnology: A Gentle Introduction to the Next Big Idea* (Upper Saddle River: Pearson Education).
- [5] Edelman A S and Cammarata R C 1996 *Nanomaterials: synthesis, properties and applications* (Bristol: Institute of Physics Publishing).
- [6] Wong K W, Zhou X T, Au F C K, Lai H L, See C S and See S T 1999 *Appl. Phys. Lett.* **75** 2918.
- [7] Gudixen M S, Laudon L J, Wang J, Smith D C and Lieber C M 2002 *Nature* (London) **415** 617.
- [8] Liu H I, Biegelsen D K, Ponce F A, Johnson N M and Pease R F W 1994 *Appl. Phys. Lett.* **64** 1383.
- [9] McIlroy D N, Alkhateeb A, Zhang D, Aston D E, Marcy A C and Norton M G 2004 *J. Phys.: Condens. Matter* **16** R415.
- [10] Tang Y H, Zhang Y F, Wang N, Lee C S, Han X D, Bello I, Lee S T 1999 *J. Appl. Phys.* **85** 7981.

- [11] Zhang H F, Wang C M, Wang L S 2002 *Nano Lett.* **2** 941.
- [12] Amelinckx S, Zhang X B, Bernaertsm D, Zhang X F, Ivanov V and Nagy J B 1994 *Science* **265** 635.
- [13] Kong X Y and Wang Z L 2003 *Nano Lett.* **3** 1625.
- [14] McIlroy D N, Zhang D, Kranov Y and Norton M G 2001 *Appl. Phys. Lett.* **79** 1540.
- [15] Zhang H F, Wang C M, Buck E C and Wang L S 2003 *Nano Lett.* **3** 577.
- [16] Zhang D, Alkhateeb A, Han H, Mahmood H, McIlroy D N and Norton M G 2003 *Nano Lett.* **3** 983.
- [17] Volodin A, Ahlskog M, Seynaeve E, Van Haesendonck C, Fonseca A and Nagy J B 2000 *Phys. Rev. Lett.* **84** 3342.
- [18] Chen X, Zhang S, Dikin D A, Ding W, Ruoff R S, Pan L and Nakayama Y 2003 *Nano Letters* **3** 1299.
- [19] Kirchhoff G 1859 *J. Reine Angew. Math.* **56** 285.
- [20] da Fonseca A F and Galvao D S 2004 *Phys. Rev. Lett.* **92** 175502.
- [21] da Fonseca A F, Malta C P and Galvao D S 2006 *J. Appl. Phys.* **99** 094310.
- [22] Wagner R S and Ellis W C 1964 *Appl. Phys. Lett.* **4** 89.
- [23] Olson W K 1996 *Curr. Opin. Struct. Biol.* **6** 242.
- [24] Tobias I, Swigon D and Coleman B D 2000 *Phys. Rev. E* **61** 747.
- [25] Coleman B D, Swigon D and Tobias I 2000 *Phys. Rev. E* **61** 759.
- [26] Fonseca A F and de Aguiar M A M 2001 *Phys. Rev. E* **63** 016611.
- [27] da Fonseca A F and de Aguiar M A M 2003 *Physica D* **181** 53.
- [28] da Fonseca A F, Malta C P and de Aguiar M A M 2005 *Physica A* **352** 547.
- [29] Manning R S, Maddocks J H and Kahn J D 1996 *J. Chem. Phys.* **105** 5626.
- [30] Goriely A and Tabor M 1998 *Phys. Rev. Lett.* **80** 1564.
- [31] McMillen T and Goriely A 2002 *J. Nonlin. Sci.* **12** 241.
- [32] Gottlieb O and Perkins N C 1999 *ASME J. Appl. Mech.* **66** 352.
- [33] Struik D J 1961 *Lectures on Classical Differential Geometry* (Cambridge: Addison-Wesley) p 1.
- [34] Dill E H 1992 *Arch. Hist. Exact. Sci.* **44** 2.
- [35] Goriely A and Shipman P 2000 *Phys. Rev. E* **61** 4508.
- [36] Landau L D and Lifshitz E M 1986 *Theory of Elasticity* (Oxford: Pergamon) p 64.
- [37] Love A E H 1934 *A Treatise on the Mathematical Theory of Elasticity* (Cambridge: Cambridge University Press) p 317.
- [38] Huang W M 2005 *Materials Science and Engineering A* **408** 136.
- [39] Goriely A and Tabor M 1996 *Phys. Rev. Lett.* **77** 3537.
- [40] Goriely A and Tabor M 1997 *Physica D* **105** 20.
- [41] Goriely A and Tabor M 1997 *Proc. Roy. Soc. London A* **453** 2583.
- [42] Salvadori M C, Brown I G, Vaz A R, Melo L L and Cattani M 2003 *Phys. Rev. B* **67** 153404.
- [43] Salvadori M C, Vaz A R, Melo L L and Cattani M 2003 *Surf. Rev. Lett.* **10** 571.
- [44] Dikin D A, Chen X, Ding W, Wagner G and Ruoff R S 2003 *J. Appl. Phys.* **93** 226.
- [45] Cuenot S, Frétiigny C, Demoustier-Champagne S and Nysten B 2004 *Phys. Rev. B* **69** 165410.